Characterization of Falcon 9 launch vehicle noise from far-field measurements

Logan T. Mathews, Kent L. Gee, and Grant W. Hart

Citation: The Journal of the Acoustical Society of America **150**, 620 (2021); doi: 10.1121/10.0005658
View online: https://doi.org/10.1121/10.0005658
View Table of Contents: https://asa.scitation.org/toc/jas/150/1
Published by the Acoustical Society of America

JASA ARTICLE

Characterization of Falcon 9 launch vehicle noise from far-field measurements[a)]

Logan T. Mathews,[b)] Kent L. Gee,[c)] and Grant W. Hart
Department of Physics and Astronomy, Brigham Young University, Provo, Utah 84602, USA

ABSTRACT:
This study investigates source-related noise characteristics of the Falcon 9, a modern launch vehicle with a high operational tempo. Empirical prediction of the noise characteristics of launched rockets has long been a topic of study; however, there are relatively few comparisons with high-fidelity, far-field data, and historical inconsistencies persist. Various quantities are considered: overall directivity, overall sound power, maximum overall sound pressure level (OASPL), and peak frequency. The noise directivity of the Falcon 9 vehicle is shown to be between two disparate ranges given in the historical literature, but the observed peak directivity angle is well represented using convective Mach number concepts. A comparison between mechanical and acoustic power yields a radiation efficiency is consistent with the literature. Two independent methods of predicting maximum OASPL produce results accurate within 2 dB, even at distances of several kilometers. Various scaling parameters are calculated for observed spectral peak frequency and connect these measurements with prior observations. Finally, the impact of terrain shielding on levels and spectra is assessed. These determined source characteristics of the Falcon 9 vehicle provide a connection to prior launch vehicle acoustics studies, which helps identify useful models and methods for understanding rocket noise. © *2021 Acoustical Society of America*. https://doi.org/10.1121/10.0005658

(Received 29 March 2021; revised 28 June 2021; accepted 1 July 2021; published online 27 July 2021)
[Editor: James F. Lynch] Pages: 620–633

I. INTRODUCTION

Predictive models for noise generated by space launch vehicles are required to determine vibroacoustic loading on vehicles, payloads, and launchpad structures. Additionally, as the numbers of launch vehicles and launch facilities grow globally, and launch frequency increases, potential environmental and community noise impacts need to be assessed. However, our understanding of the fundamental physics of rocket exhaust plumes remains limited, and to a fair extent, is based on Apollo Program-era understanding, when many experimental programs on rockets and other jets of different scales were conducted.[1–6] These studies culminated in the development of the ubiquitous 1971 NASA SP-8072 report by Eldred[7] that contains empirical methodologies for predicting the noise from rockets. Since then, attention in the launch vehicle noise community has mostly gone from fundamental physical characterization to applying empirical,[8,9] scaled experiments,[10–12] and numerical methods[13,14] to predict pad environments. Relatively few studies have returned with new experimental data from full-scale rocket measurements and vehicle launches to examine fundamental physical characteristics of the noise radiation. However, doing so allows connections to be made to both historical campaigns and experiments and more recent investigations of highly heated, supersonic jets. It also allows some physical inconsistencies present in the launch vehicle noise literature to be examined.

One notable exception to the trend of launch vehicle work is the collection of papers produced by McInerny and colleagues, who reviewed essential physical parameters associated with rocket plumes, and analyzed far-field noise waveform and spectral characteristics from post-Apollo program vehicles measured with improved hardware.[15–20] Four rocket noise characteristics that McInerny examined were (1) radiation directionality through peak directivity angle, (2) radiated overall sound power, (3) sound pressure level at the peak emission angle, and (4) scaling of spectral peak frequency. Also examined were the impact of instrumentation[21] and environmental effects (e.g., absorption, nonlinearity)[17,20] that contributed to observed spectral characteristics. Using far-field measurements, this article examines the acoustical characteristics of the Falcon 9 first-stage rocket in a similar vein to some of McInerny's work.

Some initial discussion of the different launch vehicle noise characteristics analyzed in this article is helpful. For example, directivity functions associated with rockets have been measured various times; however, attempts to reconcile measurements with physical understanding and with each other have not always been successful. Historically, large differences in directivity have been observed between horizontally fired static rockets and launched rockets. Cole *et al.*[1] showed that the peak radiation direction for launched rockets was greater by ∼20°–25°. Sutherland[22] investigated the static and launch directivities of similar large rockets

[a)]This paper is part of a special issue on Supersonic Jet Noise.
[b)]ORCID: 0000-0002-1892-3319.
[c)]Electronic mail: kentgee@byu.edu, ORCID: 0000-0002-5768-6483.

 0001-4966/2021/150(1)/620/14/$30.00

https://doi.org/10.1121/10.0005658

and found the static and launched directivities to differ by 10°. McInerny[15,19] noted this discrepancy and suggested horizontally fired static rocket directivities may be affected by ground effects not present in launch vehicle measurements and that launch vehicle measurements may have been affected by meteorological effects. Even with this inconsistency between static and launched directivities, there has been widespread variation in the reported angles of peak radiation of static rockets in the literature. Mayes *et al.*[2] (see their Fig. 11) and Potter and Crocker[6] (see their Fig. 9), found directivities to fall in the ranges of 35°–45° and 40°–55°, respectively. Curiously, Fig. 20 from a Potter and Crocker[6] report indicates an observed angle of maximum radiation much different than both of the previous figures, falling somewhere in the range of 60°–65°. This conundrum in the historical literature has not satisfactorily been resolved, but modern measurements may provide an avenue to find order.

More recently, James *et al.*[23] modeled the directivity for a horizontally fired, static reusable shuttle rocket motor (RSRM) and predicted the peak radiation angle to be somewhat between historical predictions for static and launched rockets. Because Mach wave radiation[24–26] from convectively supersonic turbulence is now believed to be the primary contributor to the overall directionality of noise from supersonic, highly heated rocket plume exhausts,[19] a physical argument was made for the observed directivity in terms of convective Mach number. The work by James *et al.*[23] was based on a large correction to a prior directivity analysis of measurements by Kenny *et al.*[27] and Haynes *et al.*;[28] this correction shifted the directivity pattern approximately 11°. Given that little other directivity data have been published in the last four decades, reconciling the directivities of static and launched rocket noise, and tying them to plume physical parameters, remains an open question.

The next topic is a rocket's radiated sound power. While the power can be calculated from measured data, e.g., from far-field directivity or near-field vector intensity measurements,[29] a model for the radiated power based solely on rocket plume characteristics is useful. Eldred[7] describes radiated power in terms of a radiation efficiency, η, with 0.5% given as the most probable value and 1% given as a conservative upper bound. Because both the mechanical power and the radiated acoustic power of a rocket can be approximated as being proportional to the cube of the exit velocity, a constant radiation efficiency appears appropriate. And while Guest[4] and Sutherland[22] considered more detailed curve fits and analyses to the available data, they ultimately concluded that $\eta \approx 0.5\%$ radiation efficiency for large rockets to be reasonable.

Connected to directivity and overall power is the overall sound pressure level (OASPL) in the maximum emission direction. McInerny[15] developed a model using launch data that connects the maximum OASPL to the overall sound power. Additionally, Greska *et al.*[30] have provided a model connecting one definition of convective Mach number tied explicitly to plume parameters with the maximum overall levels expected at a common scaled distance of 100 exit diameters. This model attempts to connect a range of jets, from laboratory-scale subsonic jets to large rockets. Such a model, if accurate, could provide a simple connection between the parameters of any given jet and the expected level.

In addition to OASPL, the peak frequency in the maximum radiation direction is also of interest. Early studies, such as by Potter and Crocker,[6] attempted to scale sound power spectra using Strouhal number-type scalings across a variety of jets. However, as noted by McInerny,[19] many of these Strouhal scalings have failed to collapse spectra across a wide variety of jets. Although sound power spectra are not considered in this article for reasons of brevity and utility, the peak frequency at the maximum angle is an acceptable substitute for two reasons: first, the relative contribution of the maximum emission angle to overall sound power, and second, the relatively slow change of peak frequency with angle make comparisons between sound power and sound pressure level peak frequency valid for this case. The comparisons help connect modern data with historical scalings and reinforce the idea that our understanding of highly heated supersonic jets is incomplete.

The remainder of this article is organized as follows. First, the series of Falcon 9 launch noise measurements are described, including trajectory, atmosphere, and topography. Next, some representative data are then shown. Analyses of directivity, overall power, maximum OASP level, and spectral peak frequency are discussed. Finally, because propagation effects can alter observations of the above source characteristics, observed terrain shielding effects are discussed. The noise source characteristics of the Falcon 9 vehicle are congruent with historical studies in some ways but the integration of trajectory, meteorology, and terrain information into these analyses helps improve quantitative analysis, including resolving the differences in directivity between modern and historical studies.

II. FALCON 9 MEASUREMENTS

A. Launch vehicle

The Falcon 9 launch vehicle is an orbital class, partially reusable, medium- to heavy-lift launch vehicle developed by Space Exploration Technologies Corp. It has been primarily used as a cargo and satellite delivery vehicle but has recently been certified as a human-rated launch vehicle to transport astronauts to low earth orbit via the Crew Dragon capsule. The Falcon 9 is a two-stage liquid-fueled rocket. The first stage is comprised of a group of nine Merlin one-dimensional (1D) engines,[31] while the second stage is powered by a single vacuum-optimized Merlin engine. Each engine is fueled by a combination of RP-1 and LOX, common rocket fuels. At sea level, each of the nine Merlin 1D first-stage engines produces a maximum thrust of 845 kN, providing a total maximum first-stage thrust of 7.6 MN. Estimated engine parameters for the Falcon 9 vehicle are given in Table I. These quantities are derived from publicly

TABLE I. Estimated rocket parameters for Merlin 1D engine (Falcon 9).

Engine Parameters for Merlin 1D (Falcon 9), $P_c = 10.8$ MPa		
T_e	Exit temperature	1786 K
T_j	Fully expanded temperature	1879 K
P_e	Exit pressure	75.8 kPa
P_j	Fully expanded pressure	101 kPa
c_e	Exit sound speed	876 m/s
c_j	Fully expanded exit sound speed	898 m/s
U_e	Exit velocity	3092 m/s
U_j	Fully expanded exit velocity	3029 m/s
M_e	Exit Mach number	3.531
M_j	Fully expanded Mach number	3.377
γ_e	Ratio of specific heats at exit	1.22
D_e	Exit diameter	0.92 m
D_j	Fully expanded diameter	0.83 m
$D_{e,\text{equiv.}}$	Equivalent exit diameter	2.76 m
D_t	Throat diameter	0.23 m
Thrust	(At sea level, each engine)	845 kN

available data of the Merlin 1D engine input into the NASA-Glenn Chemical Equilibrium Program CEA2[32] using the equilibrium flow method and are similar to the parameters listed by McInerny[19] for other rocket engines.

B. Measurement location

The Falcon 9 is currently launched from Kennedy Space Center (KSC) and the adjoining Cape Canaveral Space Force Station (CCSFS) in Florida, as well as Vandenberg Space Force Base (VSFB) in California. One way in which the launch environment at VSFB differs from that at KSC and CCSFS is the surrounding terrain. While launch locations in Florida are surrounded by flat land and ocean, the launch location at VSFB is surrounded on one side by hills and mountains and the ocean on the other. This study focuses on data measured at VSFB for three different launches of the Falcon 9 vehicle, the IRIDIUM 7 NEXT (I7N), SAOCOM 1A (S1A), and RADARSAT Constellation (RC) launches, which originated from the same launch facility.

The geometry of the launch measurement is shown in Fig. 1 where d is the radial distance from the launch facility to the measurement location, h is the rocket altitude, R is the straight line distance to the rocket at any given time, and θ is the observer angle being measured relative to the exhaust axis of the rocket. While the payloads and trajectories for each Falcon 9 launch differed slightly, the trajectory information varies by less than 5% between launches for altitude, velocity, and total distance to the vehicle within the first 100 observed seconds. The trajectory for the RC launch is shown in Fig. 2 with time annotations discussed subsequently. Most of the measurable angles (88°–10°), including the peak directivity angle, occur during the time period shown in this figure. In addition, during the first 100 s of the launch, the vehicle movement is primarily vertical so the downrange movement of the vehicle is negligible.

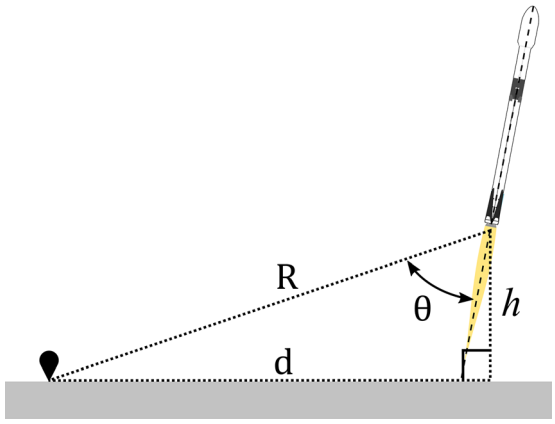

FIG. 1. (Color online) Schematic of launch vehicle measurement showing relevant dimensions.

The measurement locations were similar for all the launches measured. Most measurements were made in a flat area of fields located 6–12 km northeast of the launch facility and adjacent to the community of Lompoc. Four primary locations were used for the measurements, referred to as North Field (NF), West Field (WF), East Field (EF), and Miguelito Canyon (MC). The locations of these sites are shown in Fig. 3 and a list of locations used for each launch measurement is given in Table II. Although the number of locations utilized differed by launch, the NF location was kept consistent between launches. At the I7N and RC launch, a thick fog layer was present, while at the S1A launch, the sky was clear with no clouds or marine layer. A basic, broad analysis of all three launches and suspected meteorological effects at the NF location was presented previously by Mathews *et al.*[33]

The measurement locations differ in both their distance from the launch site and in their terrain. Elevation profiles

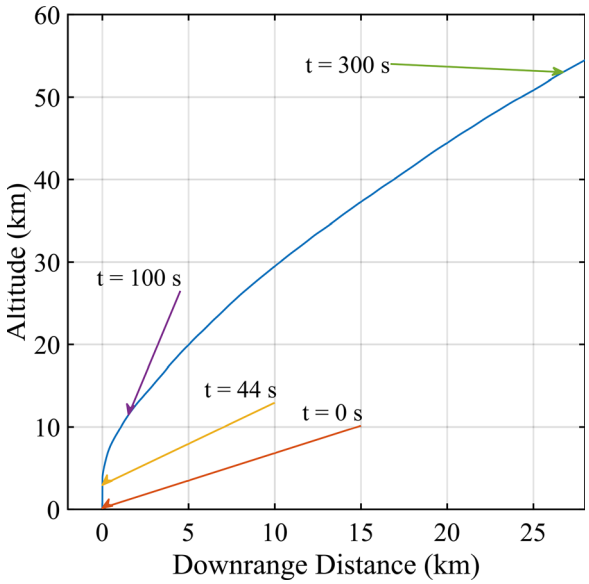

FIG. 2. (Color online) Trajectory for RADARSAT constellation launch. Time indications are shown and color coded to later figures. Indicated times reflect observation time.

https://doi.org/10.1121/10.0005658

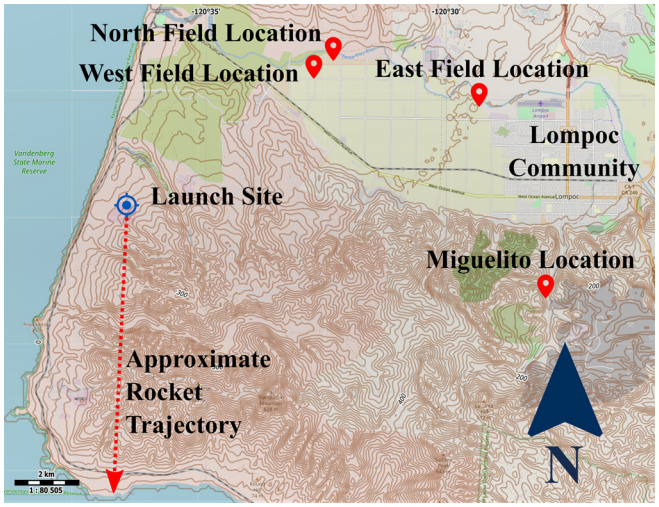

FIG. 3. (Color online) Map of measurement locations and launch site. Most measurements took place in fields west of Lompoc whereas the MC location is located south of the community and nearly due east of the launch site in significantly more complex terrain.

for the NF/WF, EF, and MC locations are shown in Fig. 4. The terrain is most similar between field locations, with terrain complexity being slightly greater at EF in contrast with the NF/WF locations. The MC location, however, has a much higher degree of terrain complexity. This results in a greater amount of terrain shielding than at any other measurement location and has the potential of creating a more reverberant environment.

C. Data acquisition

A variety of data acquisition hardware was used to produce high-fidelity recordings. Although several configurations were used at most measurement locations for comparison purposes, one configuration was kept consistent across measurements. This consisted of an NI 9234 data acquisition module and a PCB 378A07 low-frequency capable microphone placed inverted over a ground plate. Waveform data were acquired at a sampling rate of 51.2 kHz. The one exception to this is for the NF location at the RC launch, where an NI 9250 module was used to sample data from a GRAS 47AC low-frequency capable microphone in the same configuration at a rate of 102.4 kHz. The NI 9250 self-noise is lower than that of the NI 9234, but the 318A07 and 47AC microphones have similar frequency responses.

TABLE II. List of measurement locations, average radial distance to launch site, and which launches were measured at each site.

Location	d_{mean}, km	Launches
NF	8.28	I7N, S1A, RC
WF	7.34	I7N, S1A, RC
EF	11.39	RC
MC	13.68	RC

D. Assumptions

Similar to analyses previously by McInerny,[17] amplitude correction for spherical spreading is used to compare between individual sites as well as historical data. Due to the high amplitude associated with rocket noise, nonlinear propagation is expected for rockets as documented by McInerny and Ölçmen,[20] McInerny,[16] Muhlstein *et al.*,[34] and Reichman *et al.*,[35] but is not accounted for in this paper.

Some simplifications and assumptions have been made in this analysis. Due to the measurements occurring in the far field for all frequencies of concern, no corrections have been made for the source location being downstream of the rocket exit. This is an important consideration in near-field studies but becomes insignificant in the far field. James *et al.*[23] predict that the far field is approached between 200 and 300 $D_{e,\text{equiv.}}$, while McInerny[15] approximates far field behavior at $R \gg L$, where R is the distance to the source and L is the length of the source region, taken to be 30 exit diameters. In the case of these measurements, R is two orders of magnitude greater than L, and the closest measurement takes place starting at $R = 2400\, D_{e,\text{equiv.}}$, thus the far-field condition is assumed.

Additionally, the ambient sound speed changes as a function of altitude, however, a mean propagation speed of 340 m/s and straight-ray propagation is assumed. Most of the analyses of source characteristics in this paper are confined to the first 100 s of the launch when the vehicle is below 15 km in altitude. Figure 5 shows the effective sound speed profiles for all three launches at the NF location and the RC launch at all four locations, determined from radiosonde wind and temperature data collected at VSFB on the same day of each launch. The S1A launch shows the most variation, likely due to clear meteorological conditions

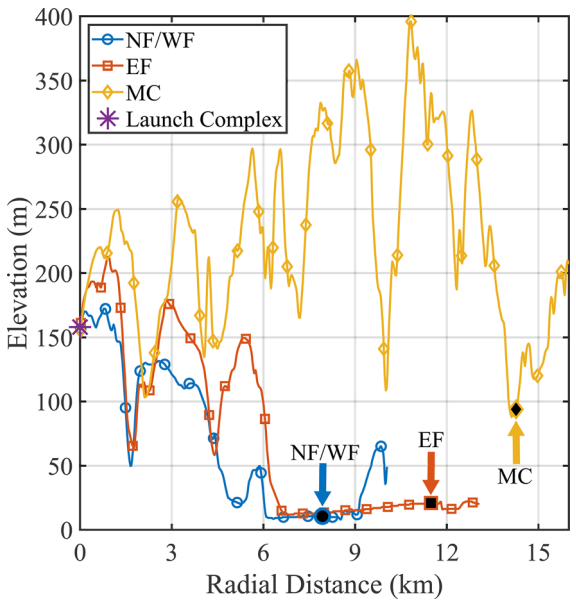

FIG. 4. (Color online) Elevation profiles for measurement locations. Approximate measurement locations are indicated by filled markers. All locations to some extent have terrain shielding during liftoff; however, the Miguelito location has significantly more terrain shielding than the field locations.

versus a heavy marine-layer fog,[33] but even so, below 5 km the sound speed is generally within ±10 m/s. A variation in the mean sound speed of ±10 m/s at peak directivity, when the vehicle is about 9 km distant and below 5 km in altitude, would result in an amplitude correction error of less than 1 dB, sufficient for our analyses. All time scales, unless otherwise noted, will be with reference to observer time.

The variations in sound speed shown in Fig. 5 do present the opportunity for atmospheric sound refraction. Refractive effects are not considered in the scope of this paper; however, investigation of refraction using ray tracing methods may provide additional insights into launch vehicle noise. Such analyses could be the subject of future work.

E. Representative data

A representative waveform from the RC launch, WF location, is shown in Fig. 6. Half-second waveform excerpts are also shown for four different time periods during the launch. These correspond to the ignition overpressure (IOP) ($t = 0$ s), near the region of peak directivity ($t = 42$ s), mid-launch ($t = 100$ s), and late-launch periods ($t = 300$ s), respectively. The location of the rocket at these time intervals is shown in Fig. 2.

The IOP is readily observable at $t = 0$ s in Fig. 6(a) as a low-frequency impulse with a peak OASPL of 102 dB. The period of the impulse is greater than that observed with other measured IOPs shown by Ryan *et al.*,[36] and the impulse is not a clean singular impulse but rather appears as a noisy impulse with many oscillations. This is likely due to obstructing terrain and launchpad scattering, but further IOP analysis is beyond the scope of this study.

The signal near peak directivity (at around $t = 42$ s) contains significant acoustic shock content as shown in Fig. 6(b). Figure 6(c) shows continued acoustic shock content at $t = 100$ s, but with reduced amplitude and lower characteristic frequencies. Figure 6(d) shows an even larger reduction in amplitude, but a relative increase in high-frequency content at $t = 300$ s. Even with the attenuation present in Fig. 6(d), there are pronounced acoustic shocks present. Considering that the waveform observed at 300 s was generated nearly 65 km distant, the presence of such pronounced shock structures is of note. Analyses of these shocks such as those performed by McInerny[16] and McInerny and Ölçmen[20] could be performed in the future.

Figure 7(a) shows the running overall sound pressure level (OASPL) from the waveform shown in Fig. 6. The block size used in the computation of running OASPL is 1 s. This figure shows both the as-measured running OASPL and the running OASPL corrected for geometric spreading based on vehicle location. Note that the amplitude-corrected OASPL flattens out after approximately $t = 100$ s, as the angle relative to the rocket plume enters the range of ±10°, approximately constant within the "cone of relative silence" region directly behind the plume.

Figure 7(b) shows spectra around each of the specified time periods computed with 4 s block sizes. The OASPL

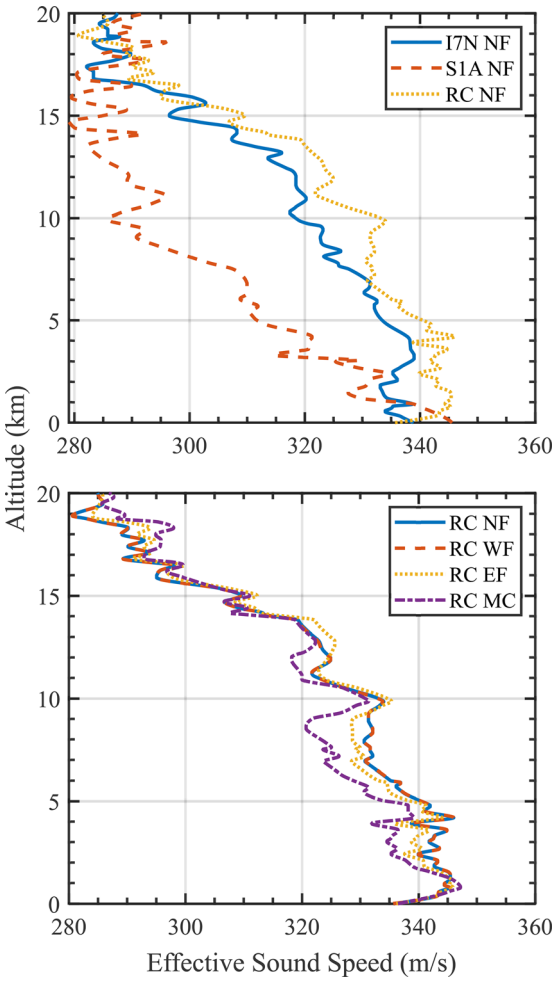

FIG. 5. (Color online) Effective sound speed profiles for (a) all three launches for the NF location and (b) for the RC launch at all four locations.

for each spectrum is reported in the legend. The spectra in Fig. 7(b) match what is qualitatively observable in the waveforms in Fig. 6. The spectrum of Fig. 7(b) (near peak directivity) contains the most high-frequency content. The peak frequency in this region is about 30 Hz. Even in the late launch phase, where $R > 64$ km for $t = 300$ s, the bandwidth of the signal is over 100 Hz. The noise floor seen in these spectra is due to the self-noise associated with the low frequency-capable measurement hardware used and is compounded in the one-third octave spectral representation. Even so, at later times in the launch [such as that shown by Fig. 6(d)], the impact of filtering out the noise floor affects OASPL values by less than 0.01 dB.

III. ANALYSIS

A. Directivity

Historical sources have shown significant variation between directivities of rockets fired in a static environment as opposed to launched vehicles. Cole *et al.*[1] observed peak radiation for launched vehicles to fall within the 70° to 80° range on average, while static peak radiation angles tended to fall within the 50° to 60° range. Eldred's[12] NASA SP-

https://doi.org/10.1121/10.0005658

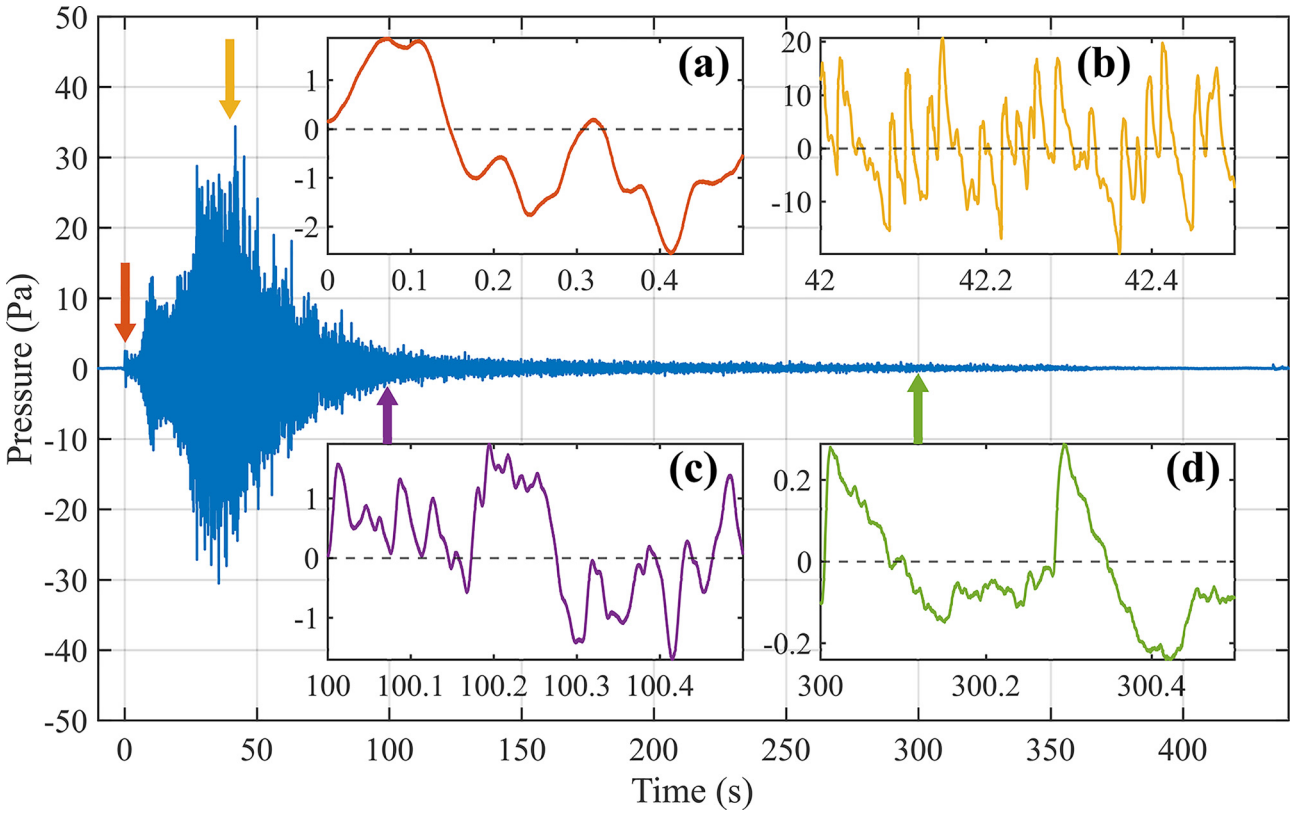

FIG. 6. (Color online) Representative waveform from the RC launch, WF location. Waveform segments of 0.5 s are shown from four different time periods during the launch. (a) Corresponds to the IOP, where a low-frequency impulse is visible. (b) Is from near peak directivity where many acoustic shocks are visible. Acoustic shocks are still present in (c) and (d), with very pronounced shock structures present in (d).

8072 document,[7] the most cited rocket noise document, shows the OASPL peaking at approximately 50° for a chemical rocket. On the other hand, James *et al.*[23] predicted a peak radiation angle for OASPL from 60° to 65° for a horizontally (static) fired RSRM, after correcting for the original source location assumption from Haynes and Kenny.[28] The Fukuda *et al.*[37] measurements of a 260 kN static solid motor show a peak directivity angle between 35° and 50°, but like the RSRM measurements, their measurements were likely not in the geometric far field.

For comparison with the historical data, Fig. 8 shows the average OASPL directivity of the Falcon 9 vehicle across all three launches. This data is the average of measurements made at two to three locations at each launch, for a total of seven distinct measurements. All OASPL curves were amplitude-adjusted for spherical spreading using the appropriate trajectory data to a common distance of 6.5 km to allow a more direct comparison. The MC location is not included due to terrain shielding during that time interval. A mean curve is shown with a shaded region corresponding to one standard deviation from the mean, showing a range of variability for the mean directivity. The median for this dataset is consistently within ±1 dB of the mean, indicating that there are not any extreme outliers. These data show an average peak radiation angle of about 64° with the 1 dB down region extending across 58° to 70°, which is much closer to the recent measurements of James *et al.*[23] for a static, high-thrust rocket than the original Cole *et al.*[1] launch measurements.

Since the peak directivity angle for rocket noise radiation is controlled by Mach wave radiation, a prediction of the angle of maximum radiation can be tied to some characteristic Mach number, as argued by McInerny *et al.*,[22] Tam,[25] and Seiner *et al.*[26] To develop such a characteristic scaling parameter, Greska *et al.*[30] proposed using a convective Mach number that Greska had previously defined and called the Oertel convective Mach number (M_{co}) in his studies of supersonic jet noise reduction. The Oertel convective Mach number is the arithmetic average of two other convective Mach numbers given by Oertel[38] in their studies of different kinds of Mach waves observed in supersonic jets. This convective Mach number is written as

$$M_{co} = \frac{U_j + \frac{1}{2}c_j}{c_j + c_a}, \tag{1}$$

where U_j is the fully expanded jet velocity, c_j is the speed of sound at the exit for the fully expanded condition, and c_a is the speed of sound in the surrounding atmosphere.

Using the approximate fully-expanded parameters for the Falcon 9 (shown in Table I), we find an Oertel convective Mach number for the Falcon 9 to be $M_{co} \approx 2.81$. This value would suggest a peak radiation angle of 69° given the relationship

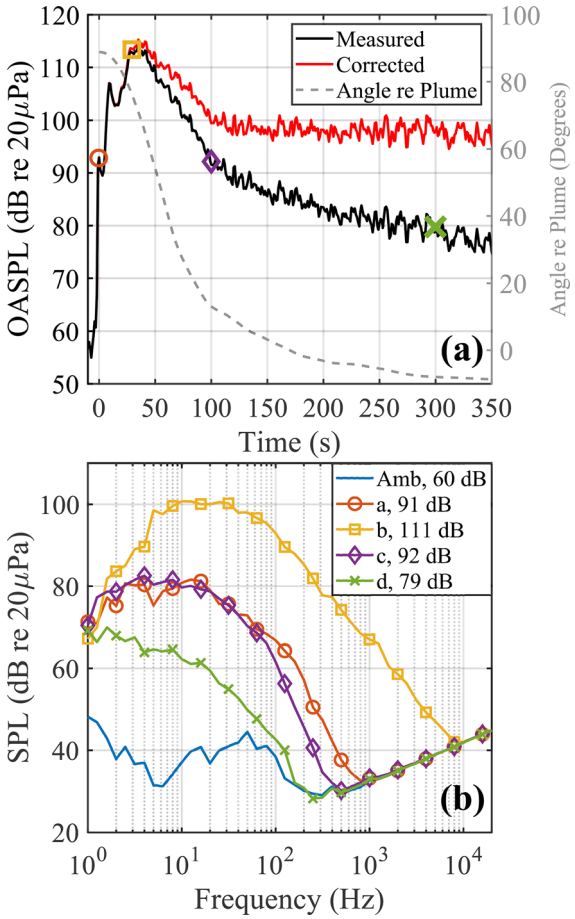

FIG. 7. (Color online) (a) OASPL as measured and corrected for spherical spreading along with approximate observer angle relative to the plume axis. (b) One-third octave spectra for the time periods in Fig. 6, along with the ambient spectrum. OASPL for each spectrum is noted in the legend.

$$\theta_{pk} = \cos^{-1}\left(\frac{1}{M_{co}}\right). \tag{2}$$

This convective Mach number was previously used by James *et al.*[23] to reconcile their predicted peak directivity angle for RSRM with the plume physics. For Falcon 9 launch data, this falls just below the lower end of maximum directivity angles for launch vehicles from Cole *et al.*[1] but is near the assumed peak directivity angle of 70° used by McInerny[15] in various far-field analyses. While the angle is about 5° higher than what we observe for the Falcon 9, it is at the top end of the 1 dB-down range.

One possible explanation for this predicted angle being greater than the observed peak directivity angle has to do with the vehicle movement. Although forward motion effects were neglected by McInerny in previous analyses,[22] the large distance at which these Falcon 9 measurements were taken causes the peak directivity angle to be measured later into the launch when the vehicle velocity becomes significant. As defined in Eq. (1), the Oertel convective Mach number using the ambient and plume parameters alone leaves out any consideration for vehicle movement. The convective Mach number attempts to describe the relative velocity at which turbulent structures in the mixing layer are convected downstream. Since the mixing layer is caused by the mixing of the high-speed rocket exhaust and "static" atmosphere, an alteration of this static condition (such as by a moving vehicle) may alter the properties of the mixing layer, and the resulting convection, ultimately reducing the effective convective Mach number. This reduction would lead to a directivity shift towards the exhaust axis, as suggested by Ribner[39] and Sutherland.[22]

While there are multiple possible methods of accounting for forward flight on convective Mach number, only the simplest correction is considered here. We propose a simple "effective" convective Mach number, $M_{\mathrm{co,eff}}$, to account for the vehicle velocity. This effective number is defined by subtracting the vehicle Mach number, M_v, from the Oertel convective Mach number, mathematically stated as

$$M_{\mathrm{co,eff}} = M_{\mathrm{co}} - M_v. \tag{3}$$

The approximate vehicle speed at the time (angle) of the measured peak level is $M_v = 0.55$ relative to $c_a = 340$ m/s. Equation (3) results in an effective convective Mach number of approximately $M_{co,eff} \approx 2.26$. This adjusted value results in a predicted θ_{pk} of 64°, in agreement with the measured peak radiation angle of 64°. Although an argument could be made for explicitly subtracting the vehicle velocity from U_j in Eq. (1), recall that the Oertel convective Mach number itself is an empirically derived number that has been found by Greska *et al.*[30] to correlate with peak OASPL. And, while the $M_{co,eff}$ results are promising in context of the measured Falcon 9 directivity here, additional studies and measurements are required to verify its transferability.

The Oertel convective Mach number is different than other convective Mach numbers used in the literature to

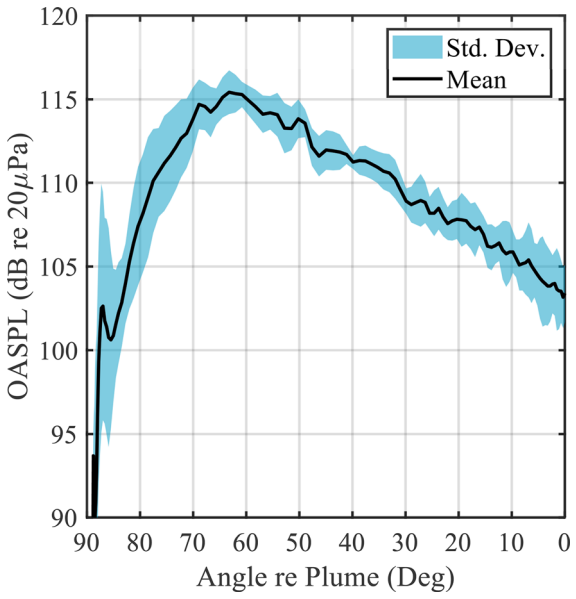

FIG. 8. (Color online) Mean OASPL as a function of angle relative to the rocket plume, corrected for amplitude to a common distance of 6.5 km. While some variation is present, the mean peak directivity angle falls within the 60° to 70° range.

https://doi.org/10.1121/10.0005658

predict θ_{pk}. One common definition for the relationship between convective Mach number and peak radiation angle for a supersonic jet is given as

$$\theta_{pk} = \cos^{-1}\left(\frac{c_a}{U_c}\right) = \cos^{-1}\left(\frac{c_a}{\kappa U_j}\right), \tag{4}$$

where U_c is a convective velocity and κ is an empirical parameter that relates a characteristic velocity (taken here to be U_j) to U_c. Values for κ range from 0.6 to 0.85 in the literature. Greska *et al.*[30] consider a typical value of 0.7; however, Tam[25] finds a value of 0.8, and Seiner *et al.*[26] favor 0.75. Assuming $\kappa = 0.7$, the predicted angle as given by Eq. (4) is 81°, which is far from the observed directivity angle for the Falcon 9 and from any directivity reported in the literature for a static rocket plume. This would suggest that typical values for κ in other supersonic jets found in the literature may be inappropriate for rockets, however, additional data from other rockets are needed to verify this finding. Taking θ_{pk} to be 69°, as calculated from M_{co} for a static Merlin 1D engine, Eq. (4) suggests $\kappa \approx 0.31$. To integrate flight effects into Eq. (4), we again subtract Mach numbers

$$\theta_{pk} = \cos^{-1}\left(\frac{1}{M_c - M_v}\right) = \cos^{-1}\left(\frac{c_a}{\kappa U_j - U_v}\right), \tag{5}$$

where U_v is the vehicle velocity. For the Falcon 9, assuming that $\kappa \approx 0.31$, $\theta_{pk} = 64°$ in flight with the velocity at peak directivity. Again, we see an approximate 5° shift in peak directivity angle, in agreement with the observed value for the directivity.

One final convective Mach number scaling is worth mentioning. In a previous paper, McInerny[19] utilizes a similar model as Eq. (4) in an analysis of launch data, but suggested that the characteristic velocity is the sound speed at the exit, c_e, instead of U_j, resulting in

$$\theta_{pk} = \cos^{-1}\left(\frac{c_a}{\kappa c_e}\right). \tag{6}$$

This model predicts a peak radiation angle of 58° with $\kappa = 0.7$ as used by McInerny.[19] Although this formulation, proposed using launch data, does not agree well with either the previous predictions of θ_{pk}, it does reflect the earlier findings of Cole *et al.*[1] for static rockets and does fall at the lower edge of the 1 dB-down directivity region of the Falcon 9.

Comparing these three methods of predicting the angle of peak radiation, the models that appear to be most reasonable in this study are those given by the effective Oertel convective Mach number from Eqs. (2) and (3) and the alternative convective Mach number in Eq. (5), provided that κ is allowed to be significantly less than what is in the literature. Since κ has been estimated through experimentation, this radically different value indicates the empirical nature of this model. Nevertheless, these two methods consider many variables related to the production of noise, including vehicle velocity; however, Eq. (5) does not account for temperature. Further investigation of this predictor of peak radiation angle may help to establish their effectiveness across a broad range of jet noise sources.

While the peak radiation angle is important, so is the angular spread of the peak radiation region. The measured 3 dB-down directivity peak for the Falcon 9 has an angular spread of about 30° on average. This is similar to the ∼30° spread shown by Kenny *et al.*[27] for a horizontally fired RSRM, the 30°–35° spread shown by Fukuda *et al.*,[37] and the ∼35° spread shown by Sutherland[22] for a launched Saturn I vehicle (comparable in scale/thrust to the Falcon 9). In addition, Cole *et al.*[1] showed an average 3-dB down angular spread of 36° for a variety of rockets. A directivity model proposed by Sutherland[22] varies significantly from the Falcon 9 directivity peak, The Falcon 9 peak is significantly smaller, with Sutherland's model having a 3 dB-down angular spread of 56°. Sutherland's model is congruent, however, with the findings of Eldred[7] for a standard chemical rocket which show a 57° 3 dB-down spread. The average OASPL angular spread for the Falcon 9 is comparable to most other measurements of static and launched vehicles, only differing with Sutherland's[22] directivity model and Eldred's[7] findings.

B. Overall sound power

The radiated sound power can be estimated from the directivity of the OASPL. Assuming azimuthal symmetry for noise radiation we can estimate the overall sound power by summing the measured intensities (obtainable from the measured far-field pressures) over a hemispherical surface, according to the method used by Matoza *et al.*[40] Azimuthal symmetry is expected given the geometric symmetry of the rocket engines on the vehicle. Using the measured directivity, the OAPWL for the Falcon 9 vehicle is calculated to be 196 dB re 1 pW. This sound power estimation includes only the rear hemisphere surrounding the vehicle (angles between 0° and 90° relative to the plume); however, due to the directivity associated with the vehicle, it is assumed that any contributions to the sound power from the front half of the vehicle will be insignificant. This assumption is further shown to be reasonable by Matoza *et al.*[40]

A mechanical-to-acoustic power radiation efficiency of 0.5% has been generally accepted for large vehicles (Eldred[7]). Based on the plume parameters in Table I, the rocket's first stage mechanical power is expected to be 11.8 GW. Assuming a 0.5% radiation efficiency, this would predict an OAPWL of 198 dB re 1 pW. This prediction falls remarkably close to the calculated sound power found from the measured and corrected OASPLs. While there is certainly room for error in these sound power calculations, this suggests that a 0.5% radiation efficiency for large rockets is reasonable as Guest[4] and Sutherland[22] have noted. The calculated OAPWL of 196 dB re 1 pW implies a radiation efficiency of 0.34%, which is less than the 0.5% favored in the historical literature. However, atmospheric losses and other attenuative effects are not considered in this analysis and may contribute to a different predicted radiation efficiency

as the measurement occurred at distances of many kilometers from the source. Nevertheless, this difference in radiation efficiency between the literature and our calculated value only results in a 2 dB difference in overall level.

C. Maximum overall level

The OASPL along the peak radiation angle is related to the directivity and overall power. As part of her far-field analyses of launch data from different vehicles, McInerny[15,19] proposed a model for maximum OASPL based on the mechanical power of the rocket, utilizing a 0.5% radiation efficiency. This gives the maximum OASPL as

$$\begin{aligned}\mathrm{OASPL}_{max} &= 10\log_{10}\left(\frac{\eta W_m}{10^{-12}\mathrm{W}}\right) \\ &\quad - 10\log_{10}(4\pi R^2) + 10\log_{10}Q(\theta_{pk}) \\ &= \mathrm{OAPWL} - 10\log_{10}(4\pi R^2) + Q', \end{aligned} \tag{7}$$

where W_m is the mechanical power of the rocket, $\eta = 0.005$ is the radiation efficiency, R is the distance from rocket to observers, and $10\log_{10}Q(\theta_{pk}) = Q'$ is the directivity factor in the direction of maximum radiation, taken by McInerny[15] from data by Cole *et al.*[1] to be 8 dB. Assuming the OAPWL to be 196 dB, this model predicts the maximum OASPL to be 144 dB, which is 1 dB higher than the average OASPL of 143 dB when scaled to 100 $D_{e,\,\mathrm{equiv.}}$.

This simple model is promising for predicting maximum OASPL purely based on knowledge of plume parameters and distance. While this analysis investigates the model as determining a maximum OASPL from a calculated OAPWL, the converse is also possible. Taking the measured $\mathrm{OASPL}_{\mathrm{max}}$ to be 143 dB at 100 $D_{e,\mathrm{equiv.}}$, Eq. (7) predicts the OAPWL to be 195 dB, only 1 dB lower than calculated from measured data. Given that the OAPWL of a rocket is a difficult quantity to estimate and efficiency models require knowledge of the rocket parameters, this model could be used to estimate the OAPWL of any rocket with the measurement of a single maximum OASPL at a known distance from the source.

While the McInerny model appears to provide a good prediction of maximum OASPL, Greska *et al.*[30] have proposed a more qualitative alternative model based upon the Oertel convective Mach number. This model, which is a curve indicating the expected relationship between M_{co} and maximum OASPL, is plotted along with supporting rocket data from Greska *et al.*[30] in Fig. 9. In addition, we add a point for a static RSRM measurement with a computed convective Mach number of $M_{co} \approx 2.30$ and an estimated peak OASPL at 100 $D_{e,\mathrm{equiv.}}$ of 142 dB from James *et al.*[23] We also add the Falcon 9 data point according to effective Oertel convective Mach number, $M_{co} - M_v$.

The fitted curve proposed by Greska *et al.*[30] seems to overestimate the calculated OASPL by about 1 dB on average for the Falcon 9 and 2 dB for the RSRM measured by Kenny *et al.*[27] This overprediction is similar to that from Eq. (6). It is remarkable that these two different methods of predicting maximum overall level are roughly equivalent and have results

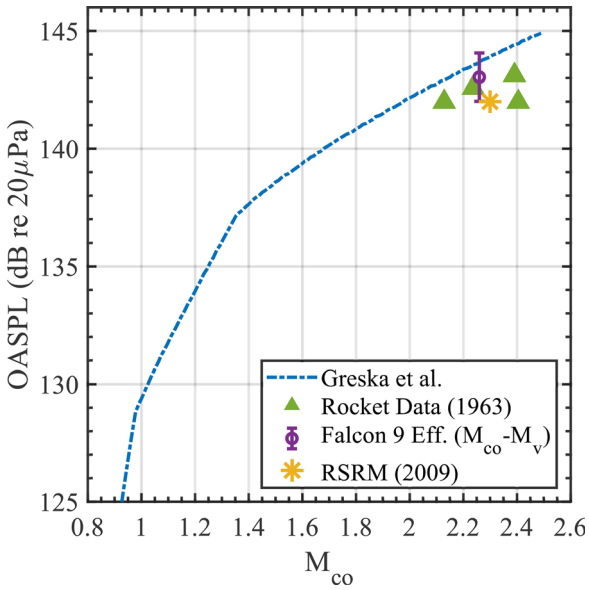

FIG. 9. (Color online) Reproduction of the model by Greska *et al.* (Ref. 30) for $\mathrm{OASPL}_{\mathrm{max}}$ as a function of M_{co} for jets of different conditions. The rocket data included by Greska *et al.* are shown, as well additional data points (RSRM and Falcon 9).

accurate within 1–2 dB given that they use two very different methods to achieve the result. The ability to use these models more broadly can be verified with additional data from other launch vehicles and from other heated, supersonic jets.

D. Peak frequency

It is well known that dominant frequency is dependent upon the scale and conditions of the noise-producing jet. Consequently, dimensionless scaling parameters are often used to connect spectra from different jets in a search for self-similarity. The difficulty lies in including all relevant physics. The dominant spectral frequency at θ_{pk} (hereafter referred to as "peak frequency" or f_{pk}) for the Falcon 9 in the far field is measured to be 21 ± 4.4 Hz on average across launches. At peak directivity, the vehicle is about $R = 9$ km distant and the signal would be expected to be of predominantly low frequencies, with some higher frequency content, which agrees with our measured peak frequency.

Various scaling parameters for frequency have been explored in the literature. Many of these parameters, such as the Lighthill parameter used by Richards and Clarkson[41] have fallen out of common use. Perhaps the most widespread scaling parameter for jet noise, used both historically and in modern studies, is the Strouhal number, which involves a frequency being multiplied by a characteristic diameter divided by a characteristic velocity. Four different Strouhal number formulations used by Eldred,[7] Cole *et al.*,[1] Greska *et al.*,[30] and Potter and Crocker[6] for rocket noise are given here (in the above order) as

$$\mathrm{Sr} = \frac{fD_e}{U_e}, \tag{8}$$

https://doi.org/10.1121/10.0005658

$$\mathrm{Sr} = \frac{fD_e}{c_e}, \tag{9}$$

$$\mathrm{Sr} = \frac{fD_e}{c_a}, \tag{10}$$

$$\mathrm{Sr} = \frac{fD_c}{c_a} = \frac{fD_t}{c_a}\sqrt{\left(\frac{2}{\gamma+1}\right)^{\gamma/\gamma-1}\frac{P_t}{P_a}}, \tag{11}$$

where f is the frequency, D_e is the exit diameter, U_e is the exit velocity, D_t is the throat diameter, γ is the ratio of specific heats in the plume, P_t is the total pressure at the throat, P_a is the ambient pressure, c_a is the speed of sound in the surrounding atmosphere, and c_e is the speed of sound at the exit. While Strouhal scalings in the historical rocket literature are applied to power level spectra, we consider their application to the sound pressure level spectrum for the Falcon 9, as the levels at θ_{pk} contributes significantly to radiated power and f_{pk} varies relatively slowly with angle. Also, because the static f_{pk} is unknown, changes in peak frequency due to forward-flight effects are unknown. However, using $M_v = 0.55$ and $\theta_{pk} = 65°$, the model of Michel and Michalke[42] suggests a downward shift in f_{pk} of about 23%, a prediction that cannot be verified here but is considered relatively minor considering that it is approximately equal to the standard deviation in measured f_{pk} (4.4 Hz).

A summary of these four different Strouhal numbers applied to the Falcon 9 vehicle is given in Table III for the equivalent diameter of the nine engines. For the Potter and Crocker formulation, an equivalent "critical" diameter was used. Equivalent diameters are given as $D_{e,\mathrm{equiv.}} = D_e\sqrt{N}$, where N is the number of engines.

The most widely applied Strouhal number across the jet noise literature is that of Eq. (8), the version used by Eldred. Variations of this Strouhal number include using the equivalent fully-expanded jet velocity in place of the standard exit velocity. For the Falcon 9, this makes little difference in the reported value. For rockets, the peak frequency for the Falcon 9 has a Strouhal number of 0.019 (from Table III). Eldred[7] and Potter and Crocker[6] reported similar values for rockets, with values from ~0.01 to 0.05. McInerny[19] later showed peak frequencies between $0.02 < \mathrm{Sr} < 0.06$ for more modern launch vehicle measurements, consistent with the historical literature. Thus, for rockets, a satisfactory collapse of peak frequency is observed. However, for other supersonic jets, Tam[24] indicates the spectral peak frequency at the maximum emission angle falls in the range $0.1 < \mathrm{Sr} < 0.3$. This appears true up through an advanced military aircraft engine at a full power set point, given that Schlinker *et al.*[43] show peak frequencies of around $0.1 < \mathrm{Sr} < 0.4$. This is approximately one order of magnitude higher than observed for rockets using the same scaling parameter. Thus, this Strouhal number seems to work well for collapsing rocket noise and other supersonic jet noise independently but does not provide a collapse across jet categories. Various scaling parameters have been proposed to address this issue.

TABLE III. Peak Strouhal numbers for various formulations are given using $D_{e,\mathrm{equiv.}}$ for the nine-engine configuration of the Falcon 9.

Strouhal Formulation	Sr ($D_{e,\mathrm{equiv.}}$)
$f_{pk}D_e/U_e$ [Eldred (Ref. 7)]	0.019
$f_{pk}D_e/c_e$ [Cole *et al.* (Ref. 1)]	0.064
$f_{pk}D_e/c_a$ [Greska *et al.* (Ref. 30)]	0.170
$f_{pk}D_c/c_a$ [Potter and Crocker (Ref. 6)]	0.250

To address the issues with the traditional Strouhal number, Cole *et al.*[1] used a slightly different formulation by taking the characteristic velocity to be c_e, as given in Eq. (9). Resulting sound power spectra are shown to peak in the range of 0.03–0.1 for rockets. The average peak frequency for rockets, turbojets, and lab-scale jets, however, falls higher at around 0.1–0.2. Thus, the collapse appears to be better than that of Eq. (8), but nonetheless, a total collapse is not achieved.

Greska *et al.*[30] investigated another alternate Strouhal scaling (specifically known as the Helmholtz number), which takes the c_a as the characteristic velocity, shown in Eq. (10). It is shown that lab-scale and rocket data converge well at the peak frequency (~1.3). For the Falcon 9, however, this formulation produces a value of 0.17, which is an order of magnitude lower. While Greska *et al.*[30] used this Strouhal scaling successfully, it does not appear to perform well outside of the data in their study. Bogey *et al.*[44] also find poor performance of the Helmholtz number for jet noise, suggesting that the fault lies with the assumption that the noise spectral characteristics are not connected to the jet velocity.

Potter and Crocker,[6] who looked at several different scalings, attempted to verify a better scaling parameter that uses a critical diameter based on engine parameters, shown in Eq. (11). This parameter was first proposed by Eldred *et al.*[45] The peak frequency range using this parameter collapses to between 0.1 and 0.5 for rockets and turbojets, as shown by Potter and Crocker[6] and McInerny.[19] For the Falcon 9, we report a value of 0.250, consistent with previous findings for rockets. This scaling method appears to perform better than the previous method, even though it still uses the ambient sound speed as the characteristic velocity.

In summary, the traditional Strouhal number [Eq. (8)] provides good collapse for similar jets but does not collapse spectra for all jet types, as differences in peak frequency for rockets and turbojets are one order of magnitude. Using c_e in place of U_e [Eq. (9)] provides a better collapse, but peak frequency still differs with jet type. Again substituting c_a for the characteristic velocity in Eq. (10) (the Helmholtz number) does not produce favorable results, but when using an adjusted diameter as shown in Eq. (11), favorable collapse is observed. Thus, Eqs. (9) and (11) are the most promising scaling parameters if collapse across all jet types is desired, but merit further investigation.

E. Spectral effects of terrain

To properly analyze spectral trends associated with rocket noise, the measured spectra need to represent the

noise generated by the rocket. In a laboratory environment, any propagation phenomena that might significantly affect the measured signal can be controlled and eliminated. This is not possible in launch vehicle measurements, however. Obstructing terrain is present in every measurement in this study. Understanding when and how terrain affects the received signal spectrally is important, but finding a simple model for the spectral effects of the terrain is even more important for application beyond this study.

Terrain shielding is readily observable when it suppresses signal levels, so we can use OASPL values to identify where terrain shielding may be present in the measurement. OASPLs are shown for the first 120 s of launch in Fig. 10. While similar behavior is visible, the MC location has significantly reduced OASPLs through the first 40–50 s of launch. This is likely attributable to terrain shielding. At this location, obstructing terrain is present between the rocket and the measurement device until the vehicle reaches an approximate height of 2.9 km, based on trajectory and topology information (see Fig. 4). This corresponds to about $t = 44$ s in the measurement. As seen in Fig. 10, the OASPL at the MC location begins to coalesce within 3 dB of the other measurements around 45 s. This is close to the predicted time of 44 s and suggests that terrain shielding is indeed the main source of sound suppression at the MC location.

Given that, at any moment during the launch, each location is at a different angle relative to the plume, this could potentially be the cause of some of the differences in levels. Quantifying the potential effects of this angular difference is therefore important if we are to assume that terrain shielding is the primary contributor to differences in overall level. As shown in Fig. 10, the angles are generally within a 10° spread during the times considered. Given that the 3 dB-down angular spread of the rocket is around 30°, the levels considered should not vary significantly due to this factor, as the shielding at the MC location is on the order of 10+ dB for most of the launch before $t = 50$ s.

An interesting phenomenon in Fig. 10 is that the levels at the MC and EF locations are higher than the other two locations after about 70 s, even though the levels are scaled to a common distance of 13.7 km. These two locations lie on different radials than that of the NF and WF locations. McInerny[19] observed atmospheric effects causing different effects on noise measured on different radials. Similar weather-based phenomena may be contributors to this difference. Further investigation of these effects may provide better justification for this observation.

Knowing the temporal region for which terrain shielding may be present at the MC location, we can investigate the spectral effects of the shielding. Figure 11 shows the one-third octave band sound pressure levels for each measured location at the RC launch. Figure 11(a) shows the spectra

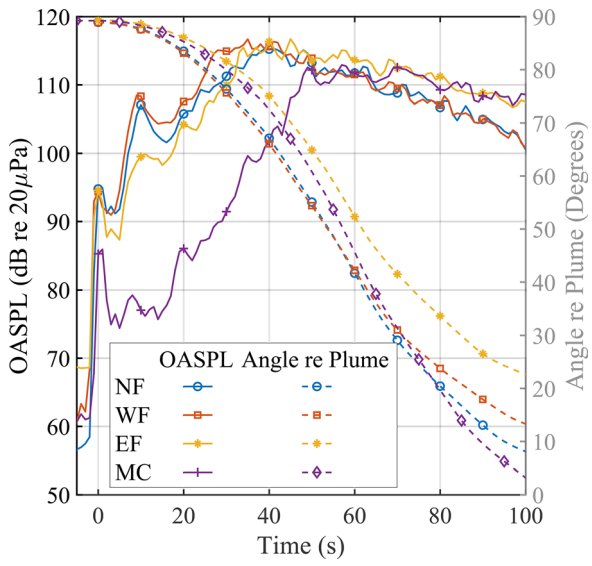

FIG. 10. (Color online) OASPLs measured during RADARSAT Constellation launch. The angle relative to rocket exhaust is also reported as a function of time. OASPLs have been scaled to a common distance of 13.7 km. Angle re plume is shown for each location without scaling.

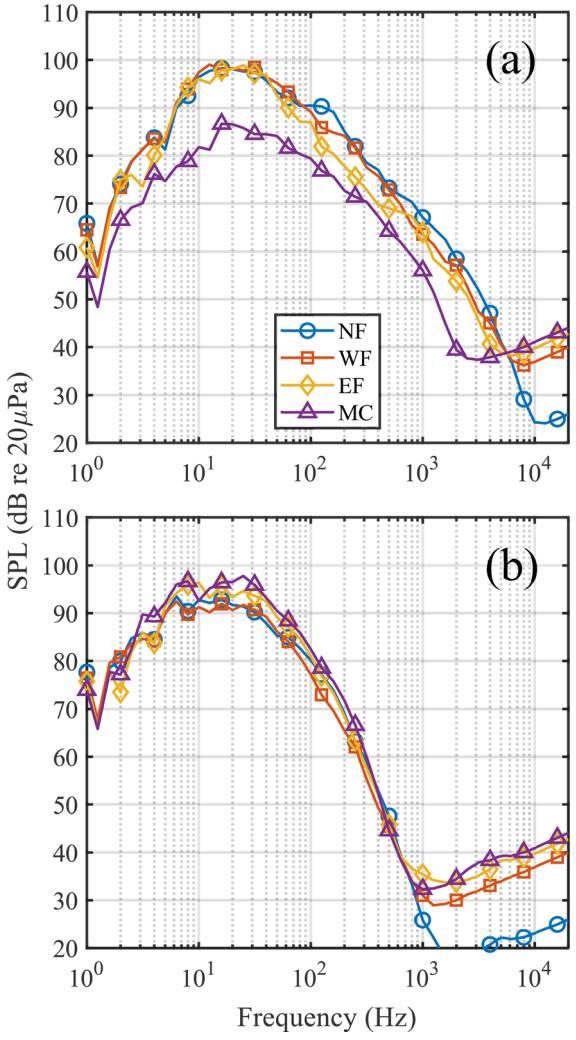

FIG. 11. (Color online) Spectra from each measurement location of RADARSAT Constellation launch, taken over 8 s windows and amplitude corrected to the average distance from the source to MC during the time period used in the spectral calculations. (a) Shows spectra from $t = 36$ s to $t = 44$ s, the approximate region of peak directivity from Fig. 7. (b) Shows spectra from $t = 56$ to $t = 64$, after line-of-sight to the vehicle is achieved at all locations.

https://doi.org/10.1121/10.0005658

from $t = 36$ to $t = 44$ s, the approximate region of peak directivity as measured at the field locations. Figure 11(b) shows spectra from $t = 56$ s to $t = 64$ s, the region for which the corrected OASPLs coalesce as seen in Fig. 10. Aside from a lower instrumentation noise floor at the NF location, the spectra reflect much of what is observable with OASPL. Band levels are overall lower for the EF and MC locations in Fig. 11(a). Overall, lower frequencies are attenuated less than higher frequencies. This is consistent with sound diffraction over a barrier, where lower frequencies are attenuated less than higher frequencies.

Figure 11(b) shows that as overall sound pressures coalesce, they do so not only in overall level but also in spectra. Even though more reverberant behavior might be expected at the MC location, the levels and spectra are similar to the other locations, suggesting any such contributions are, in fact, minor.

From terrain information, we observe that just before line of sight is achieved, only a few small obstructions are present between the rocket and the measurement location. Among these, there is one protrusion that is larger than the rest. We will therefore make a simple approximation of this obstruction as a thin barrier. The Fresnel number for such a thin barrier is given by Maekawa[46] as

$$N_1 = \frac{r_s + r_r - R_1}{\lambda/2}, \tag{12}$$

where r_s is the distance from the source to the top of the barrier, r_r is the distance from the barrier to the receiver, and R_1 is the straight-line distance from the source to the receiver. If the height of the barrier is much less than the horizontal distance from the barrier to the receiver, as would be the case with the terrain in question, we can rewrite r_r with components parallel and perpendicular to the direction of propagation, and $r_\parallel$ and $r_\perp$, respectively, as $r_r = \sqrt{r_\perp^2 + r_\parallel^2}$, and take the first order binomial expansion to find a simplified expression for the Fresnel number as

$$N_1 \approx \frac{r_\perp^2}{\lambda r_\parallel}. \tag{13}$$

Implementing this index of refraction with the thin barrier attenuation equation given by Kurze and Anderson,[47] we arrive at an equation for the approximate attenuation due to the thin barrier,

$$B_1 = 5 + 20\log_{10}\left(\frac{\sqrt{k\frac{r_\perp^2}{r_\parallel}}}{\tanh\sqrt{k\frac{r_\perp^2}{r_\parallel}}}\right). \tag{14}$$

During the time from $t = 36$ s to $t = 44$ s, the terrain shielding at the MC location can be approximated as a ~30 m tall ($r_\perp$) barrier 330 m distant ($r_\parallel$) from the measurement location. Figure 12 shows the WF and MC spectra $t = 36$ to $t = 44$, just before line of sight is achieved at the MC location. Two additional spectra are shown: one applying only geometric spreading (referred to as GS in the legend) to the WF spectrum to place it at the same distance as MC, and the other applying both geometric spreading and thin barrier shielding to the WF spectrum. Geometric spreading alone does not account for spectral differences, but when the effects of the approximated barrier are factored in the result is rather close from 1–5 Hz to 30–70 Hz. Above 70 Hz, the measured high-frequency content at the MC location is greater than that of the approximated spectrum. This may be due to nonlinear propagation, which is known to alter high-frequency energy since MC is about twice as far from the launch site as WF. Spectral effects of nonlinear propagation in rocket noise have been reported by McInerny and Ölçmen.[20] Nevertheless, the effects of terrain shielding are evident from this simple model. More advanced ray-tracing methods may produce satisfactory results for a broader range of frequencies.

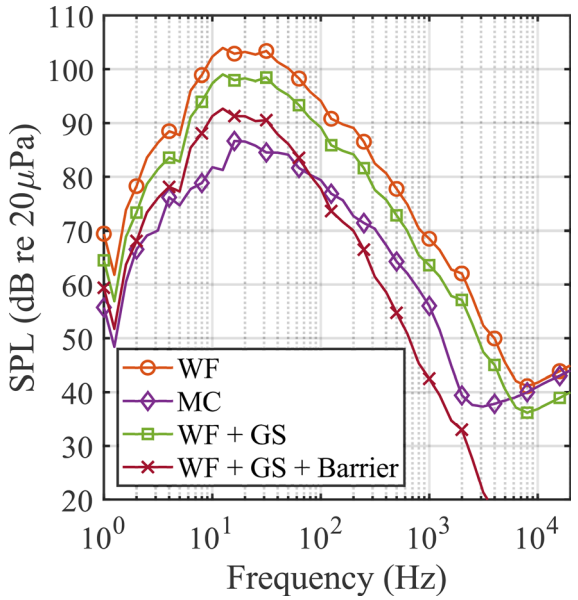

FIG. 12. (Color online) Effects of an approximated thin barrier and geometric spreading on spectra. When applying the effects of geometric spreading (noted as GS) and a thin barrier to the WF spectrum, the result is close to the MC spectrum at some frequencies.

IV. CONCLUSION

In conclusion, we have used modern, high-fidelity measurements to characterize the noise generated by the Falcon 9 launch vehicle and evaluate various models for rocket and supersonic jet noise. Similar to analyses performed by McInerny[15,19] for directivity, maximum overall level, overall sound power, peak frequency, and propagation effects, we have determined approximate source characteristics of the Falcon 9 vehicle. We have considered trajectory, meteorology, and terrain data to provide a more comprehensive analysis. The source characteristics found through these

analyses have provided increased understanding of historical discrepancies of rocket source characteristics and examined the effectiveness of various models for these characteristics.

First, the directivity of the Falcon 9 rocket is well represented by multiple convective-Mach-number-based models that incorporate flight effects. Second, the overall sound power of large rockets is verified to follow a ∼0.5% radiation efficiency model. Third, the maximum overall level is well predicted through two different empirical models. Fourth, common frequency scaling parameters fail to collapse peak frequency across many types of jets; however, variations that incorporate more characteristics of the flow produce a significantly better collapse of peak frequency. Last, the investigation of terrain shielding on spectra shows the plausibility of incorporating simple models for barrier shielding, while highlighting the likelihood of nonlinear propagation effects.

The source characteristics of the Falcon 9 rocket validate some historical models and scaling parameters, confirming some previous findings and producing new understanding of launch vehicle noise. Additional studies into these noise characteristics from static and launched rockets may produce additional evidence to finally resolve the historical discrepancies reported in the literature for rocket directivities and to improve scaling for jets across different conditions. Further work in this area can involve the consideration of atmospheric absorption, nonlinear propagation, and ray tracing models, which would certainly provide additional insight into the acoustics of the Falcon 9 vehicle.

ACKNOWLEDGMENTS

The authors would like to acknowledge the contributions of Daniel J. Novavovich, Reese D. Rasband, Aaron B. Vaughn, Pauline Nelson, and Francisco J. Irrarazabal to the measurements made in this study.

[1]J. N. Cole, H. E. Von Gierke, D. T. Kyrazis, K. M. Eldred, and A. J. Humphrey, "Noise radiation from fourteen types of rockets in the 1,000 to 130,000 pounds thrust range," WADC Technical Report No. 57, 354 (1957).
[2]W. H. Mayes, W. E. Lanford, and H. H. Hubbard, "Near-field and far-field noise surveys of solid-fuel rocket engines for a range of nozzle exit pressures," NASA Report No. TN D-21 (Langley Research Center, National Aeronautics and Space Administration, Hampton, VA, 1959).
[3]W. H. Maynes and P. M. Edge, "Noise measurements during captive and launch firings of a large rocket-powered vehicle," NASA TN D-1502 (Langley Research Center, National Aeronautics and Space Administration, Hampton, VA, 1962).
[4]S. H. Guest, "Acoustic efficiency trends for high thrust boosters," NASA TN D-1999 (George C. Marshall Space Flight Center, National Aeronautics and Space Administration, Huntsville, AL, 1964).
[5]R. N. Tedrick, "Acoustical measurements of static tests of clustered and single-nozzled rocket engines," J. Acoust. Soc. Am. **36**, 2027–2032 (1964).
[6]R. C. Potter and M. J. Crocker, "Acoustic prediction methods for rocket engines, including the effects of clustered engines and deflected exhaust flow," NASA-CR-566 (George C. Marshall Space Flight Center, National Aeronautics and Space Administration, Huntsville, AL, 1966).
[7]K. M. Eldred, "Acoustic loads generated by the propulsion system," NASA SP-8072 (National Aeronautics and Space Administration, Washington, DC, 1971).
[8]K. J. Plotkin, L. C. Sutherland, and, and B. T. Vu, "Liftoff acoustics predictions for the Ares I launch pad," in *Proceedings of the 15th AIAA/CEAS Aeroacoustics Conference (30th AIAA Aeroacoustics Conference)*, Miami, FL (May 11–13, 2009), AIAA 2009-3163.
[9]S. A. Kumar and N. Karthikeyan, "Prediction of launch vehicle noise during lift-off using a modified Eldred's method," in *Proceedings of the 14th Asian Congress of Fluid Mechanics*, Hanoi and Halong, Vietnam (October 15–19, 2013).
[10]D. D. Counter and J. Houston, "Verification of Ares I Liftoff acoustic environments via the Ares I scale model acoustic test," in *Proceedings of the 27th Aerospace Testing Seminar*, Los Angeles, CA (October 16–18, 2012), p. M12-1989.
[11]T. Ishii, S. Tsutsumi, K. Ui, S. Tokudome, Y. Ishii, K. Wada, and S. Nakamura, "Acoustic measurement of 1:42 scale booster and launch pad," Proc. Mtgs. Acoust. **18**, 040009 (2012).
[12]P. Malbéqui, R. Davy, and C. Bresson, "Experimental characterization of the acoustics of the future Ariane 6 launch pad," in *Proceedings of the 7th European Conference for Aeroacoustics and Space Science (EUCASS)*, Milan, Italy (July 3–6, 2017).
[13]S. Tsutsumi, T. Ishii, K. Ui, K. Wada, and S. Tokudome, "Study on acoustic prediction and reduction of Epsilon launch vehicle at liftoff," J. Spacecr. Rockets **52**, 350–361 (2015).
[14]J. S. West, L. L. Strutzenberg, G. C. Putnam, G. C. Liever, and, and B. R. Williams, "Development of modeling capabilities for launch pad acoustics and ignition transient environment prediction," in *Proceedings of the 18th AIAA/CEAS Aeroacoustics Conference (33rd AIAA Aeroacoustics Conference)*, Colorado Springs, CO (June 4–6, 2012), AIAA 2012-2094.
[15]S. A. McInerny, "Launch vehicle acoustics. 1—Overall levels and spectral characteristics," J. Aircr. **33**, 511–517 (1996).
[16]S. A. McInerny, "Launch vehicle acoustics. 2—Statistics of the time domain data," J. Aircr. **33**, 518–523 (1996).
[17]S. A. McInerny, J. K. Wickiser, and R. H. Mellen, "Rocket Noise Propagation," ASME Noise Control Acoust. **24**, 37–50 (1997).
[18]S. A. McInerny, G. Lu, and S. Ölçmen, "Rocket and Jet Mixing Noise, Background and Prediction Procedures," National Center for Physical Acoustics Report No. UM 03-08-013 (National Center for Physical Acoustics, University, MS, 2004).
[19]S. A. McInerny, "Characteristics and predictions of far-field rocket noise," Noise Control Eng. J. **38**, 5–16 (1992).
[20]S. A. McInerny and S. M. Ölçmen, "High-intensity rocket noise: Nonlinear propagation, atmospheric absorption, and characterization," J. Acoust. Soc. Am. **117**, 578–591 (2005).
[21]S. A. McInerny, J. K. Francine, B. S. Stewart, and P. H. Thorson, "The influence of low-frequency instrumentation response on rocket noise metrics," J. Acoust. Soc. Am. **102**, 2780–2785 (1997).
[22]L. C. Sutherland, "Progress and problems in rocket noise prediction for ground facilities," in *Proceedings of the 15th AIAA Aeroacoustics Conference*, Miami, FL (May 11–13, 1993), AIAA-93-4383.
[23]M. M. James, A. R. Salton, K. L. Gee, T. B. Nielsen, S. A. McInerny, and R. J. Kenny, "Modification of directivity curves for a rocket noise model," Proc. Mtgs. Acoust. **18**, 040008 (2014).
[24]C. K. W. Tam, "Supersonic Jet Noise," Ann. Rev. Fluid Mech. **27**, 17–43 (1995).
[25]C. K. W. Tam, "Mach wave radiation from high-speed jets," in *Proceedings of the 47th AIAA Aerospace Sciences Meeting*, Orlando, FL (January 5–8, 2009), AIAA 2009-13.
[26]J. M. Seiner, M. K. Ponton, B. J. Jansen, and N. T. Lagen, "The Effects of Temperature on Supersonic Jet Noise Emission," in *DLGR/AIAA 14th Aeroacoustics Conference*, Vancouver, BC (May 5–7, 1992), DLGR/AIAA 92-02-046.
[27]R. J. Kenny, C. Hobbs, K. Plotkin, and D. Pilkey, "Measurement and Characterization of Space Shuttle Solid Rocket Motor Plume Acoustics," in *Proceedings of the 15th AIAA/CEAS Aeroacoustics Conference (30th AIAA Aeroacoustics Conference)*, Miami, FL (May 11–13, 2009), AIAA 2009-3161.
[28]J. Haynes and R. J. Kenny, "Modifications to the NASA SP-8072 Distributed Source Method II for Ares I Lift-off Environment Predictions," in *Proceedings of the 15th AIAA/CEAS Aeroacoustics Conference (30th AIAA Aeroacoustics Conference)*, Miami, FL (May 11–13, 2009), AIAA 2009-3160.
[29]K. L. Gee, E. B. Whiting, T. B. Nielsen, M. M. James, and A. R. Salton, "Development of a near-field intensity measurement capability for static rocket firings," Trans. JSASS Aerosp. Tech. Jpn. **14**, Po_2_9–Po_2_15 (2016).

[30]B. Greska, A. Krothapalli, W. C. Horne, and N. Burnside, "A Near-Field Study of High Temperature Supersonic Jets," in *Proceedings of the 14th AIAA/CEAS Aeroacoustics Conference (29th AIAA Aeroacoustics Conference)*, Vancouver, BC (May 5–7, 2008), AIAA 2008-3026.
[31]Space Exploration Technologies Corp., "Falcon user's guide," Space Exploration Technologies Corp. (SpaceX, Hawthorne, CA, 2019).
[32]NASA Glenn Research Center, "Chemical equilibrium with applications CEARUN," https://cearun.grc.nasa.gov/ (Last date accessed: 17 Jun 2021).
[33]L. T. Mathews, K. L. Gee, G. W. Hart, R. D. Rasband, D. J. Novakovich, F. I. Irrarazabal, A. B. Vaughn, and P. Nelson, "Comparative analysis of noise from three Falcon 9 launches," J. Acoust. Soc. Korea **39**, 322–330 (2020).s
[34]M. Muhlestein, K. L. Gee, T. B. Neilsen, and D. C. Thomas, "Prediction of nonlinear propagation of noise from a solid rocket motor," Proc. Mtgs. Acoust. **18**, 040006 (2013).
[35]B. O. Reichman, B. Harker, T. Stout, E. Whiting, K. L. Gee, and T. B. Neilsen, "Acoustical measurements during a static firing of the space launch system solid rocket motor," Proc. Mtgs. Acoust. **25**, 045006 (2015).
[36]R. S. Ryan, J. H. Jones, S. H. Guest, H. G. Struck, M. H. Rheinfurth, and V. S. Verderaime, "Propulsion System Ignition Overpressure for Space Shuttle," NASA TM-82458 (George C. Marshall Space Flight Center, National Aeronautics and Space Administration, Huntsville, AL, 1981).
[37]K. Fukuda, S. Tsutsumi, K. Fujii, K. Ui, T. Ishii, H. Oinuma, J. Kazawa, and, and K. Minesugi, "Acoustic measurement and prediction of solid rockets in static firing tests," in *Proceedings of the 15th AIAA/CEAS Aeroacoustics Conference (30th AIAA Aeroacoustics Conference)*, Miami, FL (May 11–13, 2009), AIAA 2009-3368.
[38]H. Oertel, "Measured velocity fluctuations inside the mixing layer of a supersonic jet," in *Recent Contributions to Fluid Mechanics* (Springer, Berlin-Heidelberg, 1982).
[39]H. S. Ribner, "The generation of noise by turbulent jets," Adv. Appl. Mech. **8**, 103–182 (1964).
[40]R. S. Matoza, D. Fee, T. B. Nielsen, K. L. Gee, and D. E. Ogden, "Aeroacoustics of volcanic jets: Acoustic power estimation and jet velocity dependence," J. Geophys. Res.: Solid Earth **118**, 6269–6284, https://doi.org/10.1002/2013JB010303 (2013).
[41]E. J. Richards and B. L. Clarkson, "Jet and rocket noise," in *Noise and Acoustic Fatigue in Aeronautics* (Wiley, New York, 1968), Chap. 7, pp. 150–168.
[42]U. Michel and A. Michalke, "Prediction of flyover jet noise spectra from static tests," NASA-TM-83219 (National Aeronautics and Space Administration, Washington, DC, 1981).
[43]R. H. Schlinker, S. A. Liljenberg, D. R. Polak, K. A. Post, C. T. Chipman, and A. M. Stern, "Supersonic jet noise source characteristics & propagation: Engine and model scale," in *Proceedings of the 13th AIAA/CEAS Conference (28th AIAA Aeroacoustics Conference)*, Rome, Italy (May 21–23, 2009), AIAA 2007-3623.
[44]C. Bogey, S. Barré, V. Fleury, C. Bailly, and D. Juvé, "Experimental study of the spectral properties of near-field and far-field jet noise," Int. J. Aeroacoust. **6**, 73–92 (2007).
[45]K. M. Eldred, W. M. Roberts, and R. White, "Structural vibrations in space vehicles," WADD Technical Report (Wright Air Development Division, Wright-Patterson Air Force Base, OH, 1961), pp. 61–62.
[46]Z. Maekawa, "Noise reduction by screens," Appl. Acoust. **1**, 157–173 (1968).
[47]U. J. Kurze and G. S. Anderson, "Sound attenuation by barriers," Appl. Acoust. **4**, 35–53 (1971).